Energy Conversion and Management 297 (2023) 117731

Contents lists available at ScienceDirect

Energy Conversion and Management

journal homepage: www.elsevier.com/locate/enconman

Industrial cluster energy systems integration and management tool

Ugochukwu Ngwaka [a,1], Yousaf Khalid [a,1], Janie Ling-Chin [a,*], John Counsell [b], Faisal Siddiqui [c], Ruben Pinedo-Cuenca [c], Huda Dawood [c], Andrew Smallbone [a], Nashwan Dawood [c], Anthony Paul Roskilly [a]

[a] Department of Engineering, Durham University, Durham, DH1 3LE, United Kingdom
[b] Advanced Control Ltd, 54 Grange Cross Lane, Wirral CH48 8BQ, United Kingdom
[c] Centre for Sustainable Engineering, Teesside University, Middlesbrough TS1 3BX, United Kingdom

ARTICLE INFO

Keywords:
Industrial decarbonisation
Industrial cluster
Multi-vector energy systems
Renewable energy integration

ABSTRACT

Critical for achieving the United Kingdom's net-zero targets, decarbonising industrial clusters would require robust tools to assess the feasibility of decarbonisation technologies and investment solutions. This paper presents an integrated energy system planning tool for decarbonising industrial clusters. The adoption of the transfer functions method enables the development of individual component models for technologies, networks, and loads, facilitating the control and simulation of complex dynamics in multi-energy system operation, as demonstrated in a case study investigating heat and power demands of a dynamic hybrid cluster, with evaluation of decarbonisation implications including heat electrification, renewables, and fuel switching in both grid-connected and island modes to establish potential pathways for decarbonisation. With the implementation of these decarbonisation measures in the case study cluster, primary energy demand, costs, emissions, and energy losses were reduced by 42%, 71%, 53%, and 72% in grid mode and by 40%, 70%, 53%, and 63% in island mode, and higher losses in island mode is due to excess heat production by electric boilers intended to consume all available power. While outcomes might differ among various clusters due to their specific features, the study cluster, characterised by substantial heat demand compared to electricity and significant electricity exports, achieves significant emission reduction via heat electrification compared to other individual decarbonisation technology. Moreover, this tool will be instrumental in helping industrial clusters formulate comprehensive decarbonisation roadmaps based on informed decisions.

1. Introduction

The Paris Climate Accords established a global goal of limiting the temperature increase to below 2 degrees Celsius above pre-industrial levels, requiring governments and industries to adapt energy policies. The United Kingdom's (UK) Decarbonisation Strategy seeks a 78% emissions reduction by 2035 compared to 1990, aiming for net-zero emissions by 2050 [1]. The UK's industrial sector consumed 12% of energy in 2021 [2]; therefore, significant industrial decarbonisation must be met to achieve the set targets. While energy efficiency is a crucial and cost-effective decarbonisation route, its influence appears relatively modest, contributing 11% toward the 2050 emission reduction goal, compared to renewables (53%) and fuel switching (36%) [3]. Therefore, it is essential to synergise the various means available to decarbonise the industrial sector, and multiple energy systems integration (MESI) provides part of the solution. MESI enhances energy system flexibility, enabling efficient integration of intermittent renewable generation (RG), implementing energy storage technologies, reducing

Abbreviations: BHTS, Borehole thermal storage; CCGT, Combined cycle gas turbine; CE, Combustion efficiency; CHP, Combined heat and power; CO_2e, Carbon dioxide equivalent; EfW, Energy from waste; EGE, CHP electric generation efficiency; ESB, Electric steam boiler; EV, Electric vehicle; GT, Gas turbine; HOMER, Hybrid optimization of multiple electric renewables; HP, High pressure; IHP, Intermediate high pressure; LP, Low pressure; MAPE, Mean absolute percentage error; MESI, Multiple energy systems integration; NOCT, Nominal operating cell temperature; OCGT, Open cycle gas turbine; OpEx, Operating expenditure; PB, Packaged gas boiler; P2G, Power to gas; PV, Photovoltaic; PWN, Private wire network; R^2, Coefficient of determination; RG, Renewable generation; ST, Steam turbine; TGE, CHP thermal generation efficiency; TF, Transfer function.

* Corresponding author and principal investigator.
E-mail address: janie.ling-chin@durham.ac.uk (J. Ling-Chin).

[1] These two authors have made the same contribution to this study.

https://doi.org/10.1016/j.enconman.2023.117731
Received 8 May 2023; Received in revised form 6 September 2023; Accepted 1 October 2023
Available online 6 October 2023

emissions, optimising energy conversion, and providing economic benefits [4]. MESI's synergy-driven approach offers cost and efficiency advantages over individual networks [5] and accommodates RG fluctuations, enhancing RG penetration and utilisation [6].

Recent MESI studies have focused on two domains: (1) **Techno-economic and Environmental Evaluations** involving optimisation and artificial intelligence techniques to determine optimal system sizes and identify ideal combinations of MESI components to minimise emissions, costs, and energy consumption metrics [7]. (2) **MESI Assessment**, which evaluates integrated system dynamics of MESI solutions, considering uncertainties and stability [8]. The first domain conceives solutions, while the second assesses their real-world viability. Progress requires seamless digital integration of both domains, which is essential for bridging the gap between energy policy challenges, proposed solutions, and existing models' capacity to evaluate optimal MESI solutions [7]. The interest in achieving net-zero has driven the demand for MESI modelling tools that support evidence-based analysis for capital investment and emissions reduction [9]. This has highlighted the need for advanced industrial energy management systems to address integration challenges, including cross-coupled dynamical behaviours, which can cause system instabilities and suboptimal performance [10]. This study aims to create a digital tool capable of modelling cross-coupled dynamical behaviours within MESI industrial clusters, focusing on sustainable net-zero transition.

Historically, energy system modelling was closed and proprietary, prioritising intellectual property protection. However, the imperative for decarbonisation has led to increased transparency in modelling methodologies and assumptions [11]. Depending on site specifics, MESI analysis integrates various energy conversion and storage technologies, such as combined heat and power (CHP), photovoltaic (PV), batteries, heat pumps, electric vehicles (EVs), and power-to-gas (P2G), biomass [12], wind turbines, diesel engines, pumped hydro, and hydropower [13]. Colbertaldo et al. [14] presented a modelling framework encompassing multiple industrial sectors, energy technologies, energy vectors, and networks to investigate MESI. The authors used the nodal method to derive algebraic equations that model the power flow balances between each network component. The linear programming approach proposed for optimisation has potential limitations, as it requires a linearised model of the whole system, thus simplifying the cross-coupled nonlinear dynamic behaviour of MESI, which requires integration and management. The framework presented only considers cross-nodal behaviour, and data availability of each node is a challenge for meaningful evaluation of the whole network energy balance. Bechara and Alnouri [15] used a nonlinear programming approach to optimise the industrial cluster's product requirements while meeting the emission limits and maximising financial returns. The study presents an integrated model of the cluster with multiple constraints and nonlinear equations modelling the relationships of cluster parameters. This constitutes static analysis, as the optimisation occurs within a finite space defined by cluster parameters for selecting optimal fuels and configurations. Yazdani et al. [16] employed the concepts in [14] and utilised the Hybrid Optimization of Multiple Electric Renewables (HOMER) software to simulate different hybrid energy systems configurations by adjusting the component sizes to match community energy, extracting cost, power loss probability, and emissions data for each case, and subsequently, performed discrete optimisation. This optimisation type is constrained to predefined component sizes in simulated scenarios, whereas in continuous cases, the component sizes could be variable during the optimisation process. Knothner et al. [17] used discrete and continuous decision variables in a two-step approach to optimise an energy supply system to meet industrial and residential heat demand. It employed discrete variables to select the best component combinations and continuous variables for optimal component sizes. A two-step approach was used, commencing with system simulation and searching for optimal solutions using optimisation algorithms. However, dynamic simulation of optimisation cases, showing the system's transient behaviour to rapid changes or uncertainties, would help validate these approaches. The study by Prabhakaran et al. [18] integrated an MESI model with P2G plants in decentralised energy hubs. The study explores system responses to changing input parameters, emphasising interconnections and dynamic management. However, a thorough techno-economic assessment is needed to quantify sustainability metrics and make the findings actionable.

Zhang et al. [19] analysed modelling methods for integrated energy systems and identified elements of digital tools essential for designing and assessing MESI, including dynamic characteristics, operational flexibility, operation under uncertainty, reliability, system economy, and simultaneous optimisation of multiple generation resources. Several tools are available for modelling MESI, however, few tools meet the requirements highlighted in [19]. Lyden et al. [20] evaluated 51 energy system analysis tools, pinpointing 13 suitable for preliminary design analysis of community-level renewable energy and storage systems. Seven of the 13 tools lacked essential capabilities and were considered 'inadequate' whereas only HOMER offered advanced control strategies but lacked support for district heating, a critical component in industrial clusters. ReOpt conducted static analysis, omitted dynamic simulation, and disregarded energy networks as a single-node model [21]. Table 1 summarises the key features of these tools in [20], revealing that none possess the complete set of essential features for comprehensive MESI industrial cluster analysis. This study is therefore novel because the tool presented is the first with all the essential capabilities required, as outlined in the first column of Table 1, to investigate MESI.

The MESI's site-specific nature poses a primary technical barrier, limiting its applicability, especially amid uncertainty and integration challenges. Stakeholders aiming for industrial decarbonisation targets require digital tools with essential capabilities to assess and virtually commission MESI. The simulation tool described in this paper can model dynamic energy interactions in MESI across diverse industrial sites, offering comprehensive planning, operational, and management features. This tool also offers energy, cost, and emissions metrics, aiding evidence-based decision-making for energy efficiency and decarbonisation strategies, and the outcome of this study will increase knowledge of the interrelationships among multi-energy vectors within industrial clusters. A case study of an industrial cluster is conducted to analyse potential decarbonisation scenarios. The rest of this paper is organised as follows: Section 2 details modelling, simulation, and control. Section 3 introduces the industrial cluster case study, model calibration, optimisation scenarios, and results. Section 4 presents the conclusions.

2. Methods

This study applies transfer functions to model, simulate, and control industrial clusters. These functions describe energy systems and offer versatility, flexibility, and scalability in modelling. Effective modelling of MESI using transfer functions requires inputs like primary energy, system time constant, and gain (fuel conversion factor to heat and power). Interconnecting each function's output with another's input streamlines network configuration, simplifying modification. This fosters adaptable methods for diverse sites and energy setups. This generic approach ensures the tool's applicability beyond specific cases and is suitable for any industrial facility with generators, networks, loads, and storage. Given these generic components are modellable via transfer functions and are typical in most industrial sites, the transfer function method is robust for MESI modelling and simulation. The following section offers a thorough overview of the system's description, the methods utilised in model development, and the underlying assumptions. It covers various aspects, including components, networks, systems control, and simulation structure. Fig. 1 describes the methodology adopted in this study.

Table 1
Comparison of tools for modelling integrated energy systems along with essential metrics.

Tool capability	Tools												
Electrical supply	1	2	3	4	5	6	7	8	9	10	11	12	13
Biomass power plant	■	■	■	■	■	■	■	■	■	■	■	■	■
CHP	■	■	■	■	■	■	■	■	■	■	■	■	■
Grid	■	■	■	■	■	■	■	■	■	■	■	■	■
PV	■	■	■	■	■	■	■	■	■	■	■	■	■
Wind	■	■	■	■	■	■	■	■	■	■	■	■	■
Thermal supply													
CHP	■	■	■	■	■	■	■	■	■	■	■	■	■
Electric boiler	■	■	■	■	■	■	■	■	■	■	■	■	■
Fuel boiler	■	■	■	■	■	■	■	■	■	■	■	■	■
Industrial surplus	■	■	■	■	■	■	■	■	■	■	■	■	■
Waste incineration	■	■	■	■	■	■	■	■	■	■	■	■	■
District heating	■	■	■	■	■	■	■	■	■	■	■	■	■
Design optimisation													
System	■	■	■	■	■	■	■	■	■	■	■	■	■
Financial	■	■	■	■	■	■	■	■	■	■	■	■	■
Emissions	■	■	■	■	■	■	■	■	■	■	■	■	■
Results outputs													
Demand/supply matching	■	■	■	■	■	■	■	■	■	■	■	■	■
Emissions	■	■	■	■	■	■	■	■	■	■	■	■	■
Energy production	■	■	■	■	■	■	■	■	■	■	■	■	■
Financial analysis	■	■	■	■	■	■	■	■	■	■	■	■	■
Fuel consumption	■	■	■	■	■	■	■	■	■	■	■	■	■
Renewable penetration	■	■	■	■	■	■	■	■	■	■	■	■	■
Control strategies													
Advanced controls	■	■	■	■	■	■	■	■	■	■	■	■	■
Modulating output	■	■	■	■	■	■	■	■	■	■	■	■	■
Operational optimisation	■	■	■	■	■	■	■	■	■	■	■	■	■

Key: Tool features = ■ Yes = ■ No = ■
1) Biomass decision support tool; 2) COMPOSE; 3) DER-CAM; 4) EnergyPLAN; 5) EnergyPRO; 6) eTransport; 7) H2RES; 8) HOMER; 9) Hybrid2; 10) iHOGA; 11) TIMES; 12) Merit; 13) SimREN.

2.1. System description

Fig. 2 depicts a schematic representation of the proposed MESI, offering island and grid-connected modes. The cluster's energy conversion units include Combined Cycle Gas Turbine (CCGT), Open Cycle Gas Turbine (OCGT) CHP, Energy-from-Waste (EfW) CHP, Biomass CHP, Packaged Gas Boilers (PB), and industrial process heat injection. CHPs, RG, and boilers are central units integrating fuels, heat, and electricity to meet cluster heating and electricity needs. Red lines/arrows denote electricity flow, blue lines/arrows represent heat flow, and black lines/arrows indicate primary energy supply. The MESI tool can operate in heat-led and electricity-led mode.

The MESI consists of CHP units with distinct types of fuel supply to generate heat and electricity energy for the cluster. Renewable generation through PV and wind turbines are sources of additional power. The model integrated the Example Weather Year and irradiation profiles for the industrial site, using them as wind and solar data inputs. Backup heat was provided by PB and electric steam boilers (ESB), and the private wire network (PWN) managed electricity import/export from the grid. Steam at different temperatures/pressures was supplied by heat networks at dedicated property lines to meet varying heat demands. The authors adopted MESI cluster modelling methods from [22], developed in MATLAB/Simulink, to account for operational and network limitations in achieving optimal MESI. Detailed mathematical modelling and assumptions regarding generating units, electric and heat networks, and demands are presented in Sections 2.2 to 2.4.

2.2. Combined heat and power generation

The CHP plants are functionally modelled as idealised energy-based systems, represented by first-order system dynamics, which are considered sufficient for system operation and performance analysis [22]. Eqs. (1) and (2) are used to model CHP electricity and heat.

$$\dot{\chi}_{el}(t) = \dot{\chi}_{input}.\boldsymbol{EGE}.\boldsymbol{Gen}_{eff}(t) \quad 1$$

$$\dot{\chi}_{ther}(t) = \dot{\chi}_{input}.\mathbf{TGE}.\boldsymbol{Gen}_{eff}(t) \quad 2$$

where $\dot{\chi}_{el}$ is CHP power output (W); $\dot{\chi}_{input}$ is CHP energy input in fuel or thermal power (W); EGE is CHP electric generation efficiency; Gen_{eff} is CHP overall generation efficiency; $\dot{\chi}_{ther}$ is CHP thermal output (W); TGE is CHP thermal generation efficiency, $TGE = 1 - EGE - CE$; CE is combustion efficiency and in combined cycle operation, CE for the bottoming cycle equals 0.

The generator dynamics are modelled as first-order systems using Eq.

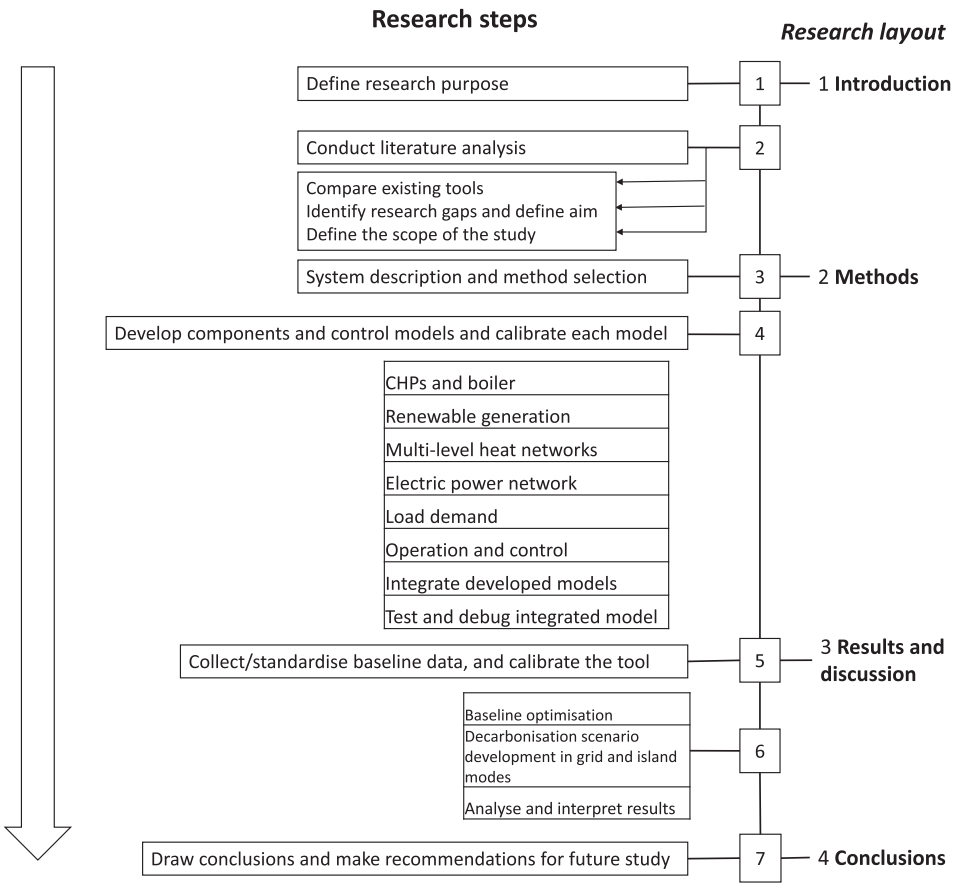

Fig. 1. The procedure employed in this study.

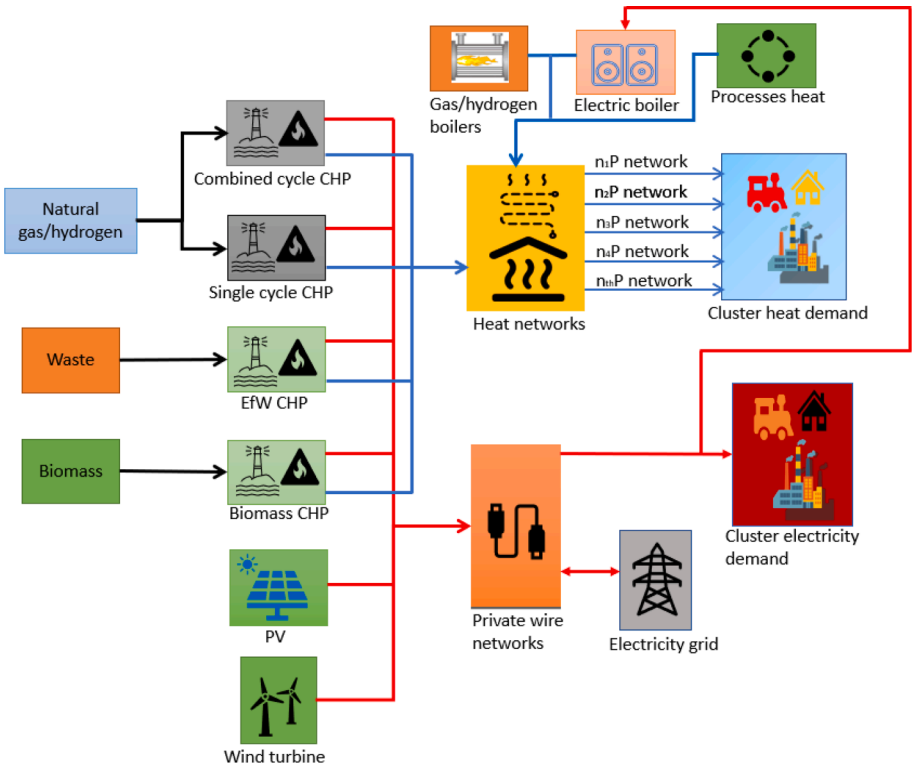

Fig. 2. Proposed multi-energy systems industrial cluster.

(3), which includes a steady-state gain and a system time constant. Eq. (4), a Laplace transform, is applied to Eq. (3), resulting in transfer functions for electricity and heat, represented by Eqs. (5) and (6), respectively [23]. Parameters for system gains and time constants are derived from Eqs. (7), (8), and (9).

$$\tau_{el}\frac{d\dot{\chi}_{el}(t)}{dt}+\dot{\chi}_{el}(t)=K_{el}\dot{\chi}_{input}(t) \tag{3}$$

$$\dot{\chi}_{el}(s)(\tau s+1)=K_{el}\dot{\chi}_{input}(s) \tag{4}$$

$$\frac{\dot{\chi}_{el}(s)}{\dot{\chi}_{input}(s)}=\frac{K_{el}}{(\tau_{el}s+1)} \tag{5}$$

$$\frac{\dot{\chi}_{ther}(s)}{\dot{\chi}_{input}(s)}=\frac{K_{ther}}{(\tau_{ther}s+1)} \tag{6}$$

$$K_{el}=\frac{EGE}{Gen_{eff}} \tag{7}$$

$$\tau_{el}=K_{fop}\frac{P_{max}}{R_{rate}} \tag{8}$$

$$K_{ther}=(1-K_{el})K_{nth},\tau_{ther}=\tau_{el}K_t \tag{9}$$

K_{el} is electrical generator gain; τ_{el} is electrical generator time constant (minutes); K_{ther} is heat generator gain; τ_{ther} is heat generator time constant (minutes); K_{nth} is a function of the number of steam outputs from the CHP and the required steam demand ratio. P_{max} is electrical capacity of power generator (MW); R_{rate} is ramp rate of electrical generator (MW/min); K_{fop} is first order system property (0.63) [23]; and K_t is thermal time factor. The CHP models feed into the steam and electrical network models described in Section 2.3.

2.3. Solar and wind power generation

Using Eqs. (10) to (13) [24], the energy delivered by the PV based on the ambient temperature and solar radiation at the study site was calculated:

$$P_{array}=\eta_p H_t A_r I_{loss} \tag{10}$$

$$I_{loss}=(1-\gamma_r)\times(1-\gamma_{pc}) \tag{11}$$

$$\eta_p=\eta_r\left[1-\beta_p(T_c-T_r)\right] \tag{12}$$

$$T_c=T_{amb}+(219+832K_t)\times\frac{(NOCT-20)}{200} \tag{13}$$

where η_p is the average array efficiency; A_r is the array area (m^2); H_t is irradiance in the plane of the PV (W/m^2); and γ_{pc} and γ_r are power conditioning and array losses, respectively; T_c is the average module temperature (K); η_r is the PV module efficiency at a reference temperature , T_r; β_p is the temperature coefficient for module efficiency. T_{amb} is the average monthly ambient temperature (K); K_t is the monthly clearness index; and *NOCT* is the Nominal Operating Cell Temperature (K).

The wind turbine electrical output, P_{el} (W), is a function of the area swept by the rotor blades, A (m^2), the wind velocity of the location, v (m/s), air density, $\rho\,(kg/m^3)$, the wind turbine performance coefficient, C_p; the global efficiency, η_g; and the gearbox efficiency, η_{gb}, as shown in Eq. (14) [25].

$$P_{el}(v)=0.5\rho A v^3 C_p\eta_{WT}\eta_{gb} \tag{14}$$

2.4. Industrial gas-fired and electric steam boilers

The PB and ESB were modelled as represented in Eq. (15), where $\dot{\chi}_b$ is the thermal output (W); $\dot{\chi}_{input}$ is the energy (electricity or gas) input (W); τ_b is the time constant; and η_b is the efficiency [26].

$$\frac{\dot{\chi}_b(s)}{\dot{\chi}_{input}(s)}=\frac{1}{(\tau_b s+1)}\eta_b \tag{15}$$

2.5. Electrical power network

The dynamic network buses, including CHP generators, demands, the grid, and future infrastructure for PV, wind, and batteries, are integrated using Kirchhoff's current law [27], as shown in Eq. (16).

$$\pm\dot{\chi}_{el\_netgrid}=\dot{\chi}_{el}+\dot{\chi}_{el\_others}-\dot{\chi}_{el\_demand} \tag{16}$$

where $\pm\dot{\chi}_{el\_netgrid}$ is the net grid import/export (W); $\dot{\chi}_{el}$ is the CHP electricity (W); $\dot{\chi}_{el\_others}$ is the electricity by other sources, like renewables (W); and $\dot{\chi}_{el\_demand}$ is the electricity demand from the users (W).

2.6. Multi-level heat network

The steam networks model relies on fundamental thermodynamic principles, and Eq. (17) provides the total heat rate transfer in the heat distribution network:

$$\dot{\chi}_{net}=\dot{\chi}_{ther}+\dot{\chi}_{process}-\dot{\chi}_{heat\_demand}-\dot{\chi}_{loss} \tag{17}$$

where $\dot{\chi}_{net}$ is the net heat transfer rate in the heat network (W); $\dot{\chi}_{ther}$ is the heat generated by the CHPs and boilers (W); $\dot{\chi}_{process}$ is the heat generated by any industrial process within the cluster and supplied to the heat network (W); $\dot{\chi}_{heat\_demand}$ is the heat demand from the cluster (W); and $\dot{\chi}_{loss}$ is the heat loss (W) through steam blow-off or expander value to lower pressure network. The pressure calculation equations for the heat networks are provided in Eqs. (18) and (19).

$$\dot{\chi}_{net}=\dot{m}c_p\Delta T\rightarrow\dot{m}=\frac{\dot{\chi}_{net}}{c_p\Delta T} \tag{18}$$

$$\frac{dP}{dt}=\frac{dm}{dt}\frac{RT}{V}=\dot{m}\frac{RT}{V}=\frac{RT}{V}\frac{\dot{\chi}_{net}}{c_p\Delta T} \tag{19}$$

where $\dot{\chi}_{net}$ is the net heat transfer rate (W); $\dot{m}$ is the steam flow rate (kg/s); c_p is the specific heat capacity of the steam (kJ/kgK); ΔT is the steam change in temperature (K); V is the volume (m^3); T is the network operating temperature (K); m is the mass of steam (kg); R is the specific gas constant (J/kgK); and P is the steam pressure (bar).

Fig. 3 shows the cluster's multi-level steam distribution network schematic, with Heat Networks 1 to n representing different pressure levels. Expander valves regulate pressures by releasing steam to lower-level networks (Option 1). The blow-off valve maintains pressure by releasing excess steam into the atmosphere (Option 2). These options can be applied at each heat network level to maintain safe pressure. Alternatively, Option 1 is used at all levels, with Option 2 applied only at the lowest level to maximise heat utilisation, as demonstrated in the case study.

2.7. Heat and power loads

This tool integrates synthetic load profiles from load models with real industrial datasets. It accommodates multiple dynamic consumer loads within each heat and power network model, as depicted in Fig. 3. It employs a hybrid approach to address data limitations and industrial process constraints, combining physics-based and measurement-based methods for modelling electricity and thermal load demands [28]. In this study, the dynamic multi-level steam and electricity demands are determined by aggregating the expected demands of individual consumers for different pressure levels and electricity. Subsequently, the heat networks and the private wire network provide these demands

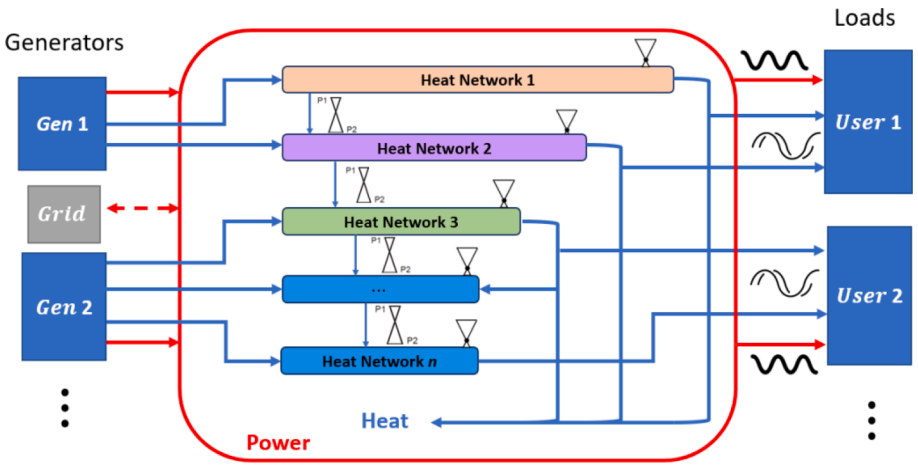

Fig. 3. Schematic of multi-level steam network with generators and demand.

accordingly.

2.8. System operation and control

Due to the intricate nature of coupled heat and power networks, diverse control strategies, both individual and centralised, were implemented as required. These strategies align with typical industrial practices and are summarised in the following subsection.

a) CHP controls regulate generation levels to maintain targeted steam pressures within the network, and this is achieved through a combination of control techniques applied to individual CHP plants:

1. Constant operating levels were adjusted by changing CHP plant capacity, as represented in Eq. (20) and Fig. 4a.
2. Timer controls that change operating levels on specified days (weekday/weekend) and season, as represented in Eq. (21) and Fig. 4b.
3. Dynamic steam supply control across various network levels and flow rates must align with consumer demands to optimise energy efficiency. The dynamic control was achieved using complex systems controllability, as shown in Eq. (22) [29] and Fig. 4c.

$$\textbf{Plant capacity},\ \mathbf{M} = \textbf{constant} \tag{20}$$

$$\mathbf{M(t)} = \mathbf{f(t)} \tag{21}$$

$$\begin{aligned} \boldsymbol{M(t)} &= \boldsymbol{f(generators,\ network\ \&\ loads\ parameters)} \\ &= \frac{\boldsymbol{RT}}{\boldsymbol{Vc_p\Delta T}}\dot{\chi}_{input}\ \boldsymbol{Gen_{eff}}\ \boldsymbol{K_{ther}}\ \dot{\chi}_{load}(t) \end{aligned} \tag{22}$$

where $\dot{\chi}_{input}$ is the generation energy input.

b) **Network pressure controls**: As the heat supply rate is varied, it is crucial to maintain the heat network's supply pressures at the specified set points to ensure a reliable supply. In cases of pressure build-up, a two-position diverter valve simulates the steam blow-off mechanism.

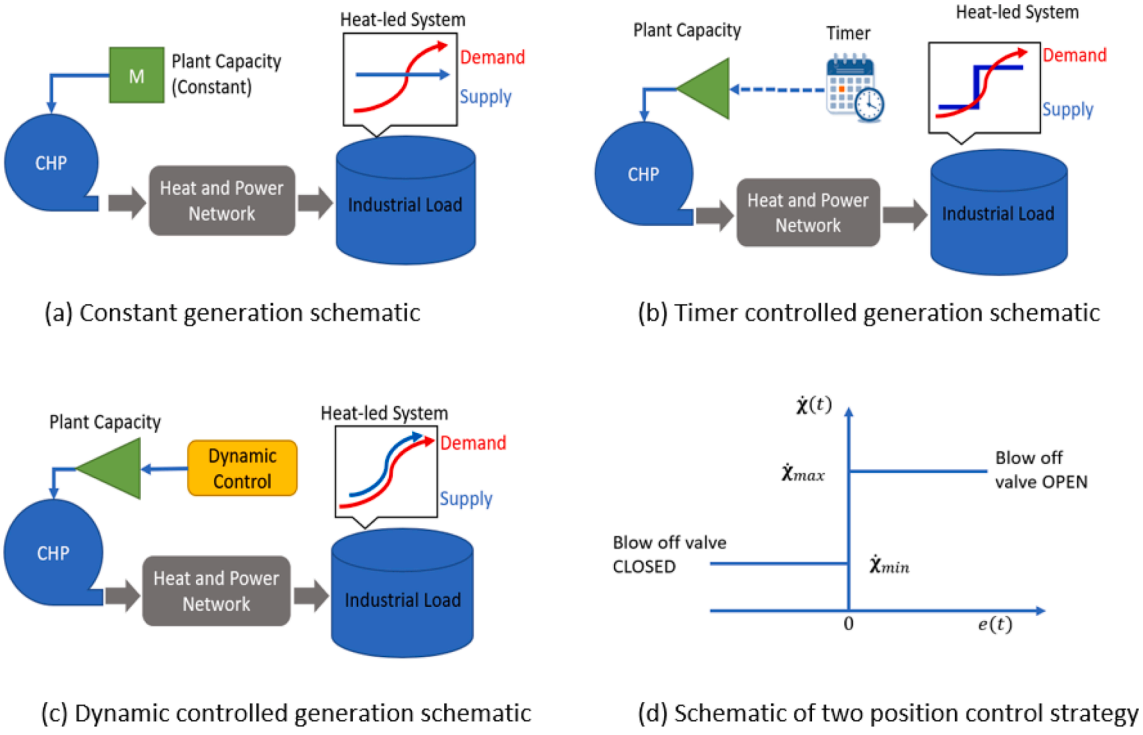

Fig. 4. Schematics of CHP generation control and two-position valve control strategy.

Set-point control was implemented as two-position control, as represented in Eqs. (23) and (24) and Fig. 4d.

$$\boldsymbol{e(t) = P_{setpoint} - P_{network}(t)} \tag{23}$$

$$\dot{\chi}_{net}(t) = \begin{cases} \dot{\chi}_{min}, & \textit{if} \quad e < 0 \\ \dot{\chi}_{max}, & \textit{if} \quad e \geq 0 \end{cases} \tag{24}$$

where $e(t)$ is the pressure difference between set-point, $P_{setpoint}$ and pipe pressure, $P(t)$; $\dot{\chi}_{net}(t)$ is the net heat going into the network; $\dot{\chi}_{min}$ is the "OFF" value or "CLOSE" blow off valve; and $\dot{\chi}_{max}$ is the "ON" value, i.e. "OPEN" blow off valve.

c) Surplus heat control: When needed, surplus heat control overrides blow-off valve operations to reduce pressure. Excess steam from higher-level networks is expanded and directed to lower-level heat networks for maximum utilisation. These connections are adaptable based on the cluster's configuration, allowing control over the ratio of multiple off-takes from a single surplus heat source. Eq. (25) represents the implementation of surplus heat control.

$$\textit{If } \boldsymbol{P(t) > P_{setpoint}}, \textit{ then } \dot{\chi}_{surplus}(t) = K_{offtake}\dot{\chi}_{net}(t) + \left(1 - K_{offtake}\right)\dot{\chi}_{net}(t) \cdots \tag{25}$$

where $\dot{\chi}_{surplus}(t)$ is the net heat flow to network (W); $\dot{\chi}_{net}(t)$ is the blow-off heat transfer; $\dot{Q}_{stX}(t)$ is the surplus heat transfer (W); and $K_{offtake}$ is the surplus heat transfer offtake factor.

In the decentralised system, prioritisation occurs: excess steam diversion takes precedence over backup boiler operation, which, in turn, supersedes central supply from primary generators. If decentralised CHP supply falls short of demand, backup boilers are activated to fill the gap, optimising energy asset integration and maximising energy efficiency and CO_2 savings.

2.9. Simulation structure

The tool's structure and simulation workflow are shown in Fig. 5a and Fig. 5b, respectively. Post-simulation, the dynamic power and heat flow, network performance, stability, and interaction with renewables and the grid are graphically displayed in the user interface at 1-minute intervals for the entire year.

3. Results and discussion

The section elaborates on the results, analyses, and discussions of model validation, optimisation of case studies, and investigation into the integration of scenario-based decarbonisation technologies in both grid-connected and island modes. The selected case study is at the integrated network level of an industry cluster comprising various sectors (e.g., steel, chemicals, pharmaceutical, food, power etc.). A facility-level investigation will be interesting and worth-investigating; however, it is different from the focus of this study and therefore it is not covered here.

3.1. Input data and tool validation

To showcase the tool's capabilities, a quad-pressure MESI industrial cluster in the UK was used for calibration and as a case study. Fig. 6 illustrates the cluster's schematic. Energy conversion systems within the cluster include CCGT CHP, OCGT CHP, EfW CHP, biomass CHP, PB, and heat injection industrial processes. Technical data for heat and electricity generation units, essential for energy integration, is summarised in Table 2. Tables 3 and 4 contain generator technical specifics and parameters for modelling equations, respectively. Heat distribution networks operate at HP 632 K, 91 bar; IHP 573 K, 67.6 bar; IP 463 K, 16.2 bar; LP 403 K, 2.2 bar. Thermal losses were accounted for; however, electrical power loss and renewable/electrical generation unit interoperability are beyond this study's scope. Fig. 7a displays the cluster's aggregated weekday electricity demand profile, while Fig. 7b depicts typical weekday, weekend, winter, and summer heat demand profiles for one facility. Fixed tariffs were adopted for primary energy supply, electricity import, and export from the grid. Natural gas, biomass, waste, electricity import, and export prices were fixed at £0.02356/kWh, £0.029/kWh, -£0.0404/kWh, £0.1438/kWh, and £0.1113/kWh, respectively. These electricity tariffs remained constant throughout the day, with waste generating revenue and the others incurring expenditure.

Information in Table 2 is sourced from the equipment's product specifications and data gathered from the cluster. The data presented in Table 3 is derived through calculations utilising Eqs. (7), (8), and (9) based on the information obtained from Table 2. The last column in Table 3 represents the steam outputs at various pressure levels from each CHP unit – a ratio that divides the total steam among different steam network pressure levels. These estimates were derived from the cluster network data.

The model validation metrics of annual primary energy and emissions were estimated through an audit of the site's existing generators. Individual facility emissions of the consumers were not considered, as it is an integrated network. Table 4 presents the primary energy demand of

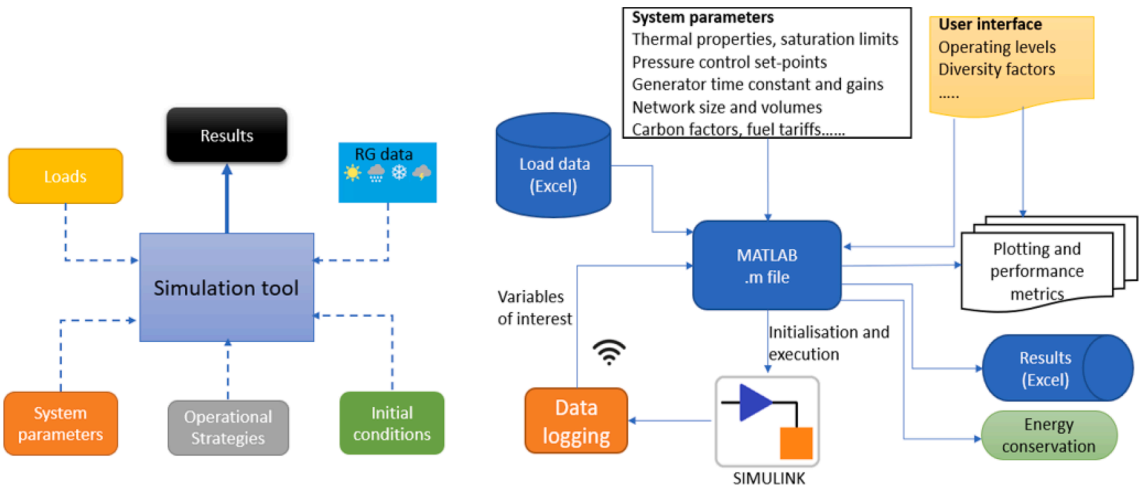

(a) High-level structure of the MES tool (b) Workflow of simulation engine

Fig. 5. High-level structure and workflow of the simulation engine.

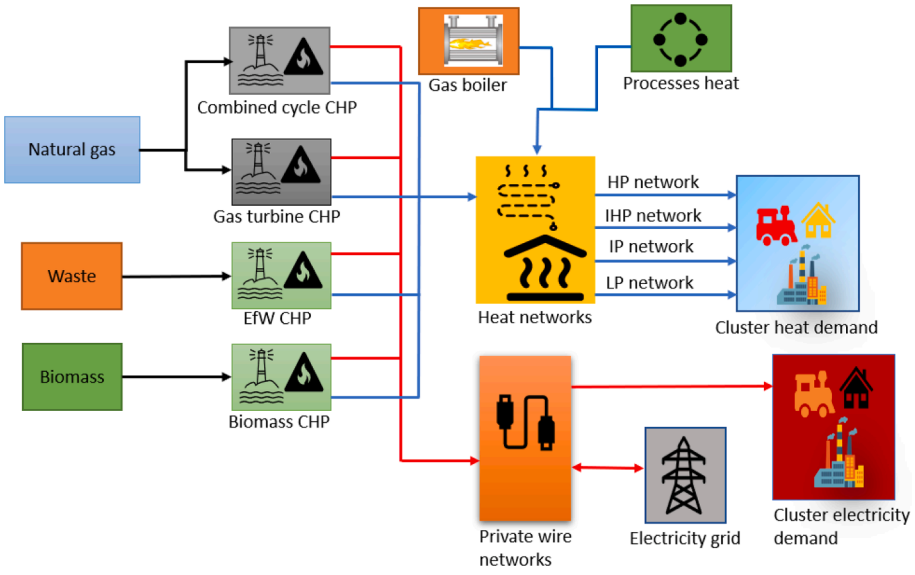

Fig. 6. Schematic of the test case MESI industrial cluster.

Table 2
Multi energy systems generation technical data.

Plant	$P_{max\_el}(MW)$	$P_{max\_ther}(MW)$	Gen_{eff}	EGE	Capacity factor	R_{rate}(MW/min)
CCGT CHPs	45 (GT) 25 (ST)	–	0.85	0.519	0.64	GT, 20; ST, 5
OCGT CHPs	40	–	0.8	0.33	0.33	20
Biomass CHPs	33	–	0.75	0.29	0.62	5
EfW CHPs	40	–	0.70	0.28	0.9	5
PB	–	120	0.85	–	0.01	–

Table 3
Parameter values of system gains and time constants.

Plant		K_{el}	K_{ther}	K_{ther2}	K_{ther3}	τ_{el}(s)	τ_{ther}(s)	K_{nth}
CCGT CHPs	GT	0.38	0.128	0.122	-	85.05	255.15	0.5 (ST) HP:0.5 HP
	ST	0.66	0.31	0.034	–	189.0	567.0	0.9 IP:0.1 LP
OCGT CHPs	0.41	0.59	–	–	75.6	226.8	1HP:0	
Biomass CHPs	0.38	0.61	–	–	249.5	748.4	1LP:0	
EfW CHPs	0.40	0.12	0.24	0.24	302.4	907.2	0.2IHP:0.4IP:0.4LP	
PB	–	1	–	–	–	300.0		

Table 4
Primary energy demand.

Primary energy	Baseline demand (GWh/year)	Model demand (GWh/year)
Natural gas (HHV)	1,338	1,339
Biomass (HHV)	619	618
Waste	1,128	1,126
Electricity exports	648	650.7
Electricity imports	0	0
Total electricity	1,016	1,083
R^2 and MAPE	0.996973 and 1.24%	

the baseline annual data (second column), the annual data predicted by the tool (third column), as well as the mean absolute percentage error (MAPE) and the coefficient of determination R^2 calculated between these datasets. The carbon intensity factors of the fuels used in the simulation and the yearly emissions results of the primary energy supply for the baseline and simulation are shown in Table 5. The user interface screenshot in Fig. 8 presents baseline calibration results. Deviations in baseline and simulated total and exported electricity may arise from unaccounted electrical losses, generation auxiliary loads, and variable factors like generation unit availability and facility load utilisation. The model assumed 70% average electricity utilisation within the cluster, with 60% exported, suggesting a heat-led operation. At this export rate, annual steam production by CHPs and boilers would be 1,146 GWh, while industrial processes generate 18.3 GWh. Actual electrical load and steam demand would amount to 432.3 and 951.3 GWh/year, respectively. The predicted annual primary energy demand, emissions and OPEX (cost of primary energy only) were 3,083 GWh, 1,148.23 $ktCO_2e$ and £76.4 million, respectively. As detailed in the following section, these indicators and the electrical and heat demands were used to further assess the tool's functionality, including its integration with RG, hydrogen, and electrifying heat.

The results in Fig. 8 indicate high heat loss in the cluster because the CHP plants operate consistently without modulation with the real-time dynamic demand, leading to surplus steam production. The K_{nth} value (refer to Table 3) is set to fulfil the maximum demand of each heat network. There needs to be automation for the heat networks. Demand was projected by the utility department (usually over-estimated) to manage supply whilst many facilities within the cluster operate below full capacity, and the heat networks operate independently. In this study, as presented in Sections 3.2 and 3.3, optimisation is achieved by modulating CHP plants' steam production and PB units' steam production to enhance cost, carbon, and energy by aligning the cluster's heat

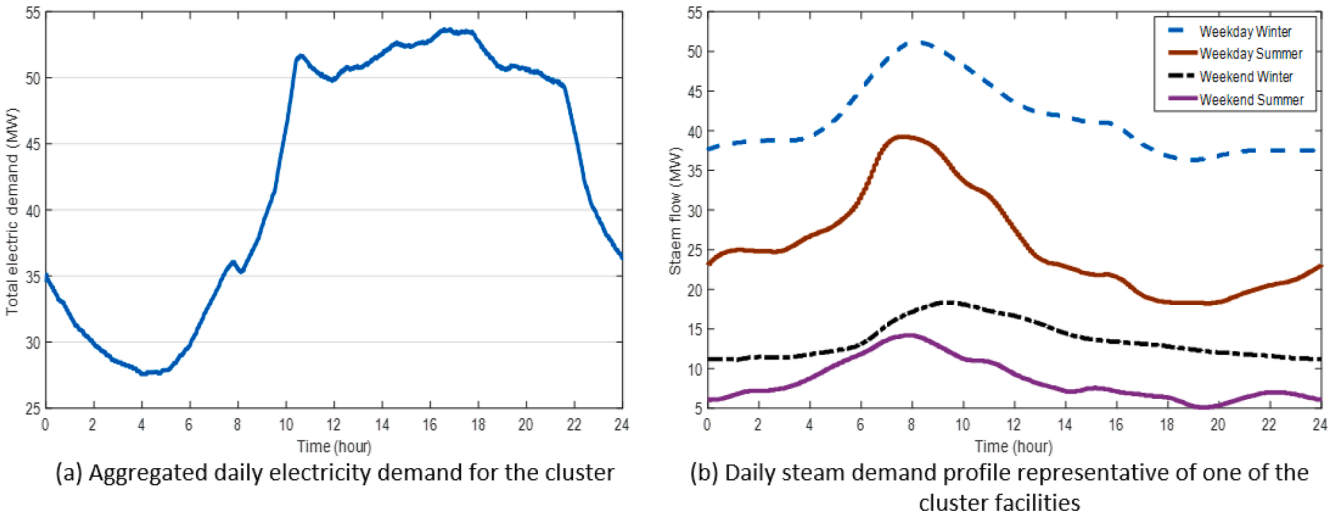

(a) Aggregated daily electricity demand for the cluster

(b) Daily steam demand profile representative of one of the cluster facilities

Fig. 7. Aggregated electricity demand and steam demand profile representative.

Table 5
Annual emissions of primary energy supply.

Baseline emissions	Carbon intensity input in the model ($kgCO_2$/kWh)	Baseline ($ktCO_2e$/year)	Model ($ktCO_2e$/year)
Natural gas	0.18 [30]	240.84	241.25
Biomass	0.01513 [30]	9.37	9.35
Waste	0.797 [31]	899	897.4
Electricity imports	0.21233 [30]	–	–
Total		1,149.37	1,148

supply with demand through dynamic CHP and PB timing control.

3.2. Optimising baseline for different objectives

Using the baseline configuration in Table 2 and the same heat and power profiles, operational and control designs with varied optimisation goals, such as energy efficiency, primary energy cost, and emissions reduction, were assessed. Table 6 displays the optimisation results in comparison to the baseline. With fewer emissions as the objective, results suggest that maintaining CCGT and EfW CHPs for baseload generation and using Biomass, GT, and PB for peak load generation on weekdays while employing CCGT for baseload and GT, Biomass, and PB for peak load on weekends, leads to a 21.7% annual emissions reduction, saving 250.2 kt of CO_2e. This approach also lowers annual energy costs and primary energy usage by 36.4% (£27.8 million) and 21.8% (673.3 GWh), respectively, while boosting energy efficiency by 12.4%. Because of grid connectivity, annual electricity imports and exports total 5.6 GWh and 372.1 GWh, respectively. The conversion unit optimally tracks cluster heat demand, leading to a reduction in heat loss. About 2.5 GWh of heat was lost annually through blow-off in emissions optimised operation compared to over 3.8 GWh, 34.1 GWh and 213 GWh in the primary energy optimisation case, energy cost optimisation case and the baseline, respectively. Additionally, grid interactions fluctuate based on CHP power generation relative to cluster power demand. When CHPs produce less power than needed, electricity is imported from the grid, and vice versa, contrasting the baseline, which only exports power to the grid.

The primary energy use was lower in cost and primary energy optimisation cases compared to the emissions and energy efficiency case, mainly due to higher grid electricity imports in the former. For cost and primary energy objectives, grid imports were 30.3 GWh and 62.1 GWh, respectively, whereas it was only 5.6 GWh for emissions and energy efficiency. Consequently, the total energy input to meet cluster demand was 2,393.8 GWh, 2,343.4 GWh, and 2,415.3 GWh for these cases if the fact that electricity is a more refined form of energy is neglected. Moreover, cost, primary energy, and emissions and energy efficiency cases exported approximately 339.4 GWh, 345.5 GWh, and 372.1 GWh, respectively, back to the grid. Compared to the primary energy input in all cases, the export in the cost-focused case was low due to the high-capacity use of EfW generation, resulting from the lower combustion efficiency of waste fuel compared to natural gas and biomass. This negatively impacted the EfW plant's generation efficiency. Energy

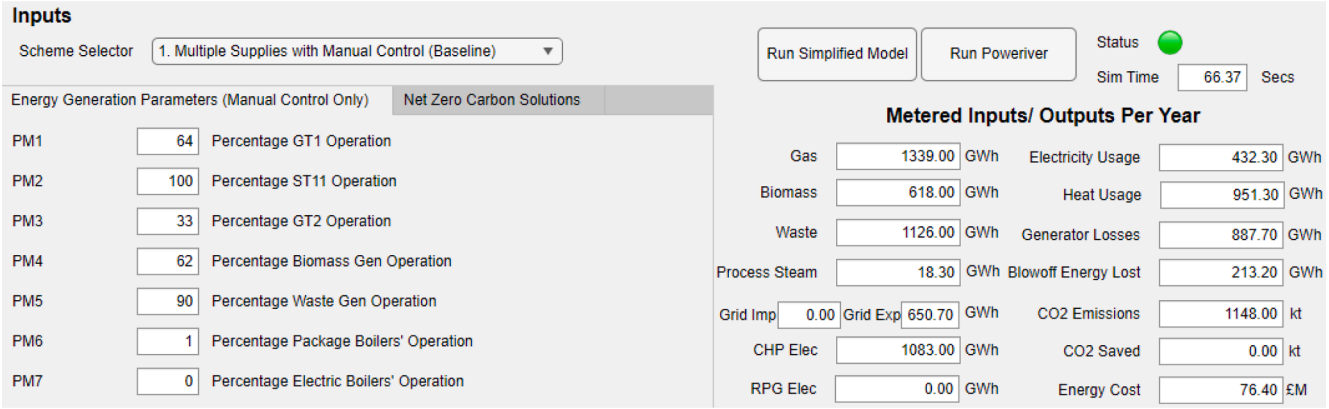

Fig. 8. Tool display for baseline validation result.

Table 6
Generator configurations for different optimisation objectives of the baseline, including energy efficiency, energy cost, primary energy usage or emission reduction.

Parameter	Baseline	Energy cost [a]	Primary energy [b]	Emissions & energy efficiency [c]
Primary energy (GWh)	3,083	2,363.5	2,281.3	2,409.7
Energy efficiency (%)	64.5	70.7	71.1	72.5
Energy cost (£million)	76.4	26.5	41.5	48.6
Emissions (kt)	1,148	1,104	978.9	897.8
Blow-off losses (GWh)	213.2	34.1	3.6	2.5
Grid imports (GWh)	0	30.3	62.1	5.6
Grid exports (GWh)	650.7	339.4	345.5	372.1

[a] Weekday: baseload generation for CCGT & EfW; and peak load generation for Biomass, OCGT & PB. Weekend: baseload generation for EfW and peak load generation for Biomass, OCGT & PB.
[b] Weekday: baseload generation for CCGT & EfW; and peak load generation for Biomass, OCGT & PB. Weekend: baseload generation for 50% EfW and peak load generation for Biomass, OCGT & PB.
[c] Weekday: baseload generation for CCGT & EfW; and peak load generation for Biomass, OCGT & PB. Weekend: baseload generation for CCGT and peak load generation for Biomass, OCGT & PB.

efficiency in all three cases was similar, ranging from 70.7% to 72.5%. The primary contributors to this efficiency were energy loss due to blow-off and the combustion efficiency of the primary energy sources, as observed in both cost and primary energy-focused cases. In the emissions and energy efficiency objective, fewer emissions resulted from using less waste fuel, with higher carbon intensity, and more natural gas and biomass, with less severe carbon intensity. In the cost objective case, 1,126 GWh of waste fuel was used, generating more revenue than the primary energy and emissions objective cases, where 948 GWh and 805.5 GWh of waste were used, respectively.

3.3. Decarbonisation interventions

Decarbonisation technology models, like RG, ESB, and hydrogen fuel switching, were added to the baseline cluster model with the same electricity and heat demands (951.3 GWh and 432.3 GWh annually). To assess RG's effectiveness under realistic conditions, conservative parameter estimates were employed, including 20% efficiency for PV, 30 m blade radius for wind turbines, and coefficients of performance, generator efficiency, and gearbox mechanical efficiency set at 0.35, 0.6, and 0.95, respectively. ESB supplied only to IP and LP networks, whereas CHPs supplied all heat networks. The study assumed a fixed number of 260 wind turbines with 0.15 MW capacity each and 10 MW PV installations. Both grid-connected and island modes for heat-led operations were evaluated in assessing decarbonisation measures. To address excess electricity production, which increased operating expenses, electrified heating was introduced to utilise surplus electricity and reduce electricity export costs. RG was integrated with electrified heating, and 20% of natural gas was replaced with hydrogen. These interventions were carried out using the same conversion unit configuration as the optimised emissions and energy efficiency objective (referred to as Case 1 in Section 3.3.1) for subsequent comparison of results.

3.3.1. Grid-connected operation

Table 7 summarises the outcomes of grid-connected and heat-led operations. Electrified heating reduced primary energy demand by 20.5% (493.3 GWh), cutting emissions by 34.3% (309.2 ktCO2e) and saving costs by 62.8% (£30.5 million) compared to Case 1, while

Table 7
Conversion units' configurations for heat-led grid mode with optimised baseline, electrifying heat, RG and 20% hydrogen.

Parameter	Case 1 [a]	Electrifying heat [b]	Electrifying heat and RG [c]	Electrifying heat, RG with 20% hydrogen [c]
Primary energy (GWh)	2,409.7	1,916.4	1,774.9	1,774.9
Energy efficiency (%)	72.5 [d]	72.2 [e]	78 [e]	78 [e]
Energy cost (£million)	48.6	18.1	14.3	21.7
Emissions (kt)	897.8	588.6	571.5	529.1
Blow-off losses (GWh)	2.5	1.8	58.3	58.3

[a] Weekday: baseload generation for CCGT & EfW; and peak load generation for Biomass, GT & PB. Weekend: baseload generation for CCGT; and peak load generation for Biomass, GT & PB.
[b] Weekday: baseload generation for CCGT & EfW; and peak load generation for Biomass, GT & PB. Weekend: baseload generation for 65% CCGT; and peak load generation for Biomass, GT & PB.
[c] Weekday: baseload generation for CCGT & EfW; and peak load generation for Biomass, GT & PB. Weekend: baseload generation for 60% CCGT; and peak load generation for Biomass, GT & PB.
[d] Calculation of energy efficiency is based on the ratio of electricity produced through primary energy (used + exported) + heat usage to the primary energy input + imported electricity.
[e] Calculation of energy efficiency is based on the ratio of electricity used since there was no export + heat usage to the primary energy input + imported electricity, without considering the impact of RG; if RG is integrated, this is because some RG would go into electric demand and some into heat demand and it is impossible to track.

importing 3 GWh of grid electricity annually. This process had two primary effects. First, it decreased the primary energy demand by allowing the ESB to utilise an excess of 265.5 GWh of surplus electricity, reducing the primary energy needed. Second, it led to stable generator efficiency by minimising the need for peak-load generators to operate under part-load conditions.

RG integration contributed 189.1 GWh of electricity. Combining electrified heating with RG further reduced primary energy demand by 7.4% (141.5 GWh), increased energy efficiency and blow-off losses, and lowered energy costs and emissions. Fig. 9 illustrates grid interaction with RG during winter and summer, with electricity import limited to weekends. Fig. 10 and Fig. 11 present cluster heat demand and supply data with and without RG integration. RG integration led to surplus heat generation, causing increased energy loss due to steam blow-off, as shown in Fig. 11. Since there were no energy storage systems, most RG powered the ESB; this integration acted as a second-layer control in heat-led operations, reducing the load on traditional generators. However, controlling surplus heat remained challenging due to RG's high fluctuations, unmatched by traditional generators' ramp rates. Blending 20% green hydrogen with natural gas saved 42.4 $ktCO_2e$ but increased energy costs due to the higher hydrogen price.

3.3.2. Island mode and heat-led operation

The results of island mode and heat-led operations, shown in Table 8, exhibited higher energy costs, emissions, and lower energy efficiencies than grid-connected operations. Despite these differences, island operations shared similar characteristics with grid-connected ones, as discussed in Section 3.3.1. Energy losses were notably significant in island operations due to the absence of grid import/export. Generators worked more to meet electricity and heat demands, resulting in surplus steam production and less efficient energy utilisation, particularly on summer weekends, as illustrated in Fig. 12. The electricity-to-heat demand ratio

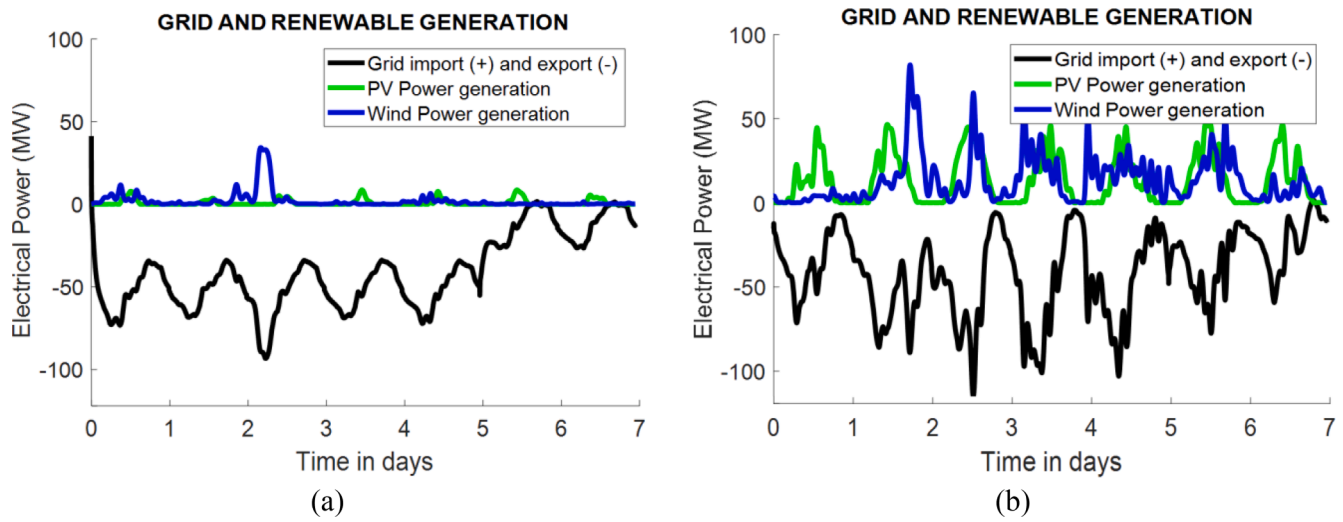

Fig. 9. Weekly grid interaction with RG for (a) winter and (b) summer conditions.

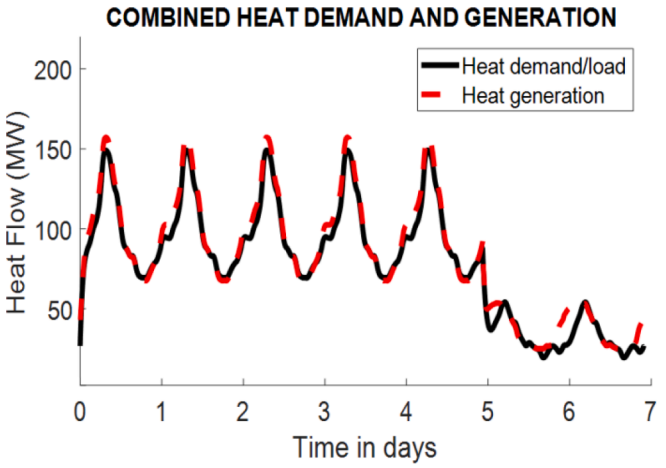

Fig. 10. Grid-connected heat demand and generation without RG for summer conditions.

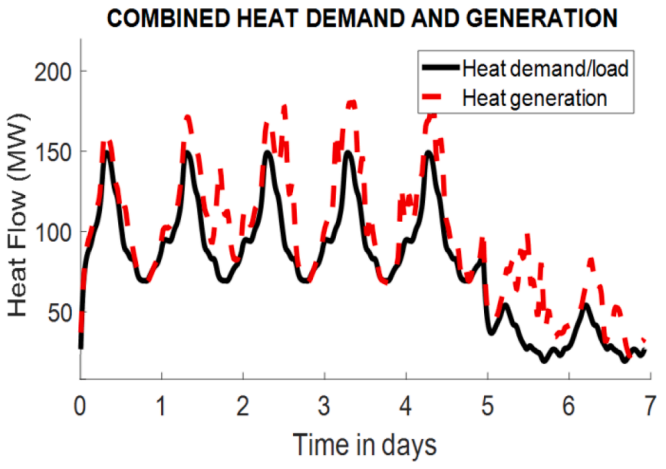

Fig. 11. Grid-connected heat demand and generation with RG for summer conditions.

varied between seasons and consistently favoured weekends over weekdays; this led to increased heat losses on weekends, contributing to the lower energy efficiency observed in island mode compared to grid-connected mode. The integration of RG worsened blow-off heat losses due to excess heat production, similar to the behaviour seen in grid-connected operations, as depicted in Fig. 13 compared to Fig. 14.

Table 8
Heat-led island mode comparison with baseline.

Parameter	Case 1 [a]	Electrifying heat [b]	Electrifying heat and RG [c]	Electrifying heat, RG with 20% hydrogen [c]
Primary energy (GWh)	2,409.7	1,948.5	1,825.4	1,825.4
Energy efficiency (%)	72.5 [d]	71 [e]	76 [e]	76 [e]
Energy cost (£million)	48.6	18.3	15.1	22.9
Emissions (kt)	897.8	595.4	583.4	538.4
Blow-off losses (GWh)	2.5	11.1	76.8	76.8

[a] Weekday: baseload generation for CCGT & EfW; and peak load generation for Biomass, GT & PB. Weekend: baseload generation for CCGT; and peak load generation for Biomass, GT & PB.
[b] Weekday: baseload generation for CCGT & EfW; and peak load generation for Biomass, GT & PB. Weekend: baseload generation for 75% CCGT; and peak load generation for Biomass, GT & PB.
[c] Weekday: baseload generation for CCGT & EfW; and peak load generation for Biomass, GT & PB. Weekend: baseload generation for 65% CCGT; and peak load generation for Biomass, GT & PB.
[d] Calculation of energy efficiency is based on the ratio of electricity produced through primary energy (used + exported) + heat usage to the primary energy input + imported electricity.
[e] Calculation of energy efficiency is based on the ratio of electricity used since there was no export + heat usage to the primary energy input + imported electricity, without considering the impact of RG; if RG is integrated, this is because some RG would go into electric demand and some into heat demand and it is impossible to track.

3.4. Implications

The case study omitted energy storage due to a consistent surplus of power exported to the grid, surpassing expectations even after careful CHP operation optimisation. The cluster meets its power needs without using the grid, except on weekends. Therefore, battery storage would undergo only one charging cycle, remaining charged without discharge

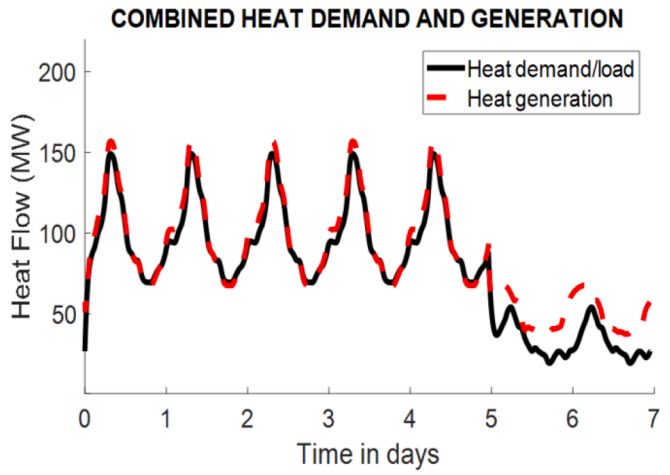

Fig. 12. Island operation heat demand and generation without RG for summer conditions.

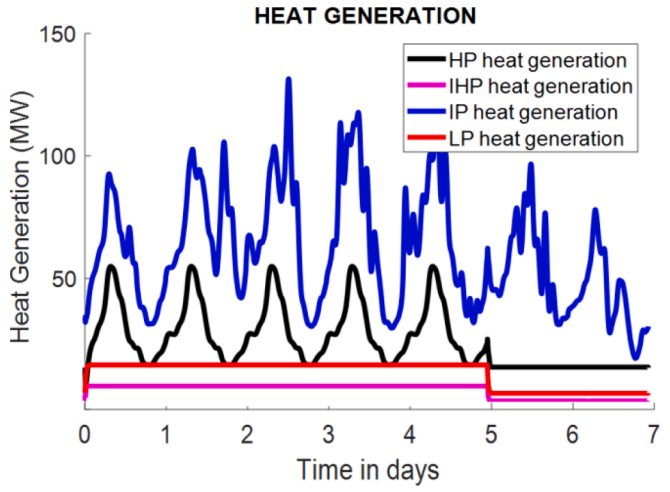

Fig. 13. Island mode heat generation for various heat networks with RG integration, summer condition.

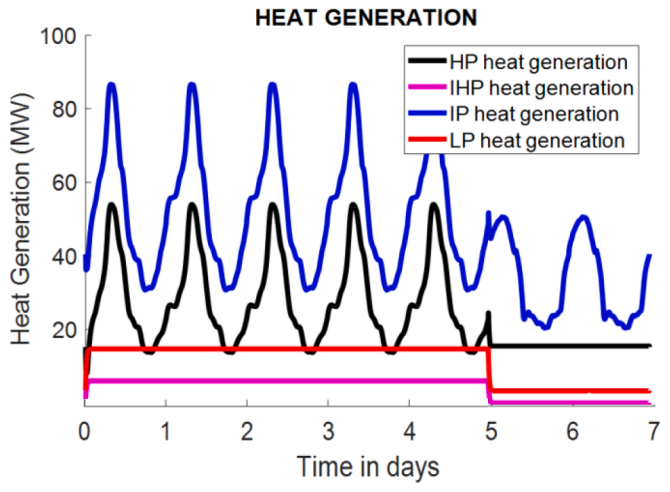

Fig. 14. Island mode heat generation for various heat networks without RG integration, summer condition.

until the weekend. The results demonstrate the tool's capability to model various cluster configurations realistically, providing essential metrics for strategic planning and investment decisions. Initially, the baseline case was compared to the results of three optimisation objectives (Table 6), revealing significant improvements in energy efficiency and emissions reduction by adjusting generator operations. Optimisation for weekends and weekdays led to 95% savings in blow-off losses and reduced primary energy demand by 25%. Reallocating generators based on demand profiles further enhanced overall efficiency by 10%, lowering emissions and blow-off losses by 22% and 95%, respectively. The introduction of ESB (Tables 7 and 8) allowed the cluster to consume surplus electricity, reducing costs by 75%, emissions by 50%, and blow-off losses by over 95%. When the cluster operates in a heat-led island mode, generation capacities are optimised for full on-site power utilisation. Integrating RG and ESB increases blow-off losses due to the overproduction of heat because generators must run at minimum capacities to maintain network pressures. A 20% blend of green hydrogen with natural gas reduces emissions by a similar value but raises costs due to higher hydrogen tariffs.

4. Conclusions

Industrial clusters are vital hubs for advancing decarbonisation, driven by the need to achieve net-zero emissions; assessing suitable decarbonisation pathways will require innovative tools. This study developed a tool to evaluate decarbonisation options for multi-energy systems industrial clusters. Utilising a case study cluster, the results of emissions optimisation demonstrated reductions in costs by 37%, losses by 95%, emissions by 21%, and a 12% increase in energy efficiency and integrating electrified heating and renewable generation in grid mode reduced, costs, emissions, and losses by 80%, 49%, and 72%, respectively. The tools need further development into an advanced integrated cluster model capable of incorporating water networks and other storage technologies. Integration algorithms, especially those containing discontinuity detection, face instability risks with larger models due to the intricate implementation demands of physics within Simulink. Despite this, MATLAB/Simulink remains a choice for developing such tools, offering swift model generation for proof-of-concepts before commercialisation as standalone software. The techniques adopted in the study are based on approaches used in aircraft flight control systems. This knowledge has expanded to multi-vector energy systems control and could apply to other systems with interconnected components. This study's findings will increase understanding of the interrelationships among multi-energy vectors within industrial clusters, and the tool will aid in formulating sustainable decarbonisation plans.

Declaration of Competing Interest

The authors declare that they have no known competing financial interests or personal relationships that could have appeared to influence the work reported in this paper.

Data availability

Data will be made available on request.

Acknowledgements

The authors thank UK Research and Innovation (UKRI) for sponsoring this research as part of Industrial Decarbonisation Research and Innovation Centre (Reference: EP/V027050/1). The project titled is "An integrated energy system planning tool for net zero industrial clusters", also referred to as Multidisciplinary Integrated Programme 1.1 or MIP1.1.

References

[1] Climate Change Committee. The sixth carbon budget: the UK's path to net zero. 2020. [cited 2023 5 May]; Available from: https://www.theccc.org.uk/wp-content/uploads/2020/12/The-Sixth-Carbon-Budget-The-UKs-path-to-Net-Zero.pdf.

[2] Department for Business, Energy and Industrial Strategy (BEIS) U. UK Energy in Brief 2022. 2022. [cited 2023 5 May]; Available from: https://assets.publishing.service.gov.uk/government/uploads/system/uploads/attachment_data/file/1130451/UK_Energy_in_Brief_2022.pdf.

[3] Mier M, Weissbart C. Power markets in transition: Decarbonization, energy efficiency, and short-term demand response. Energy Econ 2020;86:104644. https://doi.org/10.1016/j.eneco.2019.104644.

[4] O'Malley M, Kroposki B, Hannegan B, Madsen H, Andersson M, D'haeseleer W, et al. Energy Systems Integration: Defining and Describing the Value Proposition. 2016. Doi: 10.2172/1257674.

[5] Hu Y, Bie Z, Ding T, Lin Y. An NSGA-II based multi-objective optimization for combined gas and electricity network expansion planning. Appl Energy 2016;167:280–93. https://doi.org/10.1016/j.apenergy.2015.10.148.

[6] Tang C, Gu C, Li J, Dong S. Optimal operation of multi-vector energy storage systems with fuel cell cars for cost reduction. IET Smart Grid 2020;3:794–800. https://doi.org/10.1049/iet-stg.2020.0110.

[7] He Y, Guo S, Dong P, Lv D, Zhou J. Feasibility analysis of decarbonizing coal-fired power plants with 100% renewable energy and flexible green hydrogen production. Energy Convers Manag 2023;290.. https://doi.org/10.1016/j.enconman.2023.117232.

[8] Savvidis G, Siala K, Weissbart C, Schmidt L, Borggrefe F, Kumar S, et al. The gap between energy policy challenges and model capabilities. Energy Policy 2019;125:503–20. https://doi.org/10.1016/j.enpol.2018.10.033.

[9] Manuel SD, Floris T, Kira W, Jos S, André F. High technical and temporal resolution integrated energy system modelling of industrial decarbonisation. Advances in Applied Energy 2022;7. Doi: 10.1016/j.adapen.2022.100105.

[10] Rae C, Kerr S, Maroto-Valer MM. Upscaling smart local energy systems: A review of technical barriers. Renew Sustain Energy Rev 2020;131:110020. https://doi.org/10.1016/j.rser.2020.110020.

[11] Pfenninger S, DeCarolis J, Hirth L, Quoilin S, Staffell I. The importance of open data and software: Is energy research lagging behind? Energy Policy 2017;101:211–5. https://doi.org/10.1016/j.enpol.2016.11.046.

[12] Diyoke C, Ngwaka U, Onah TO. Comparative assessment of a hybrid of gas turbine and biomass power system for sustainable multi-generation in Nigeria. Sci Afr 2021;13:e00899.

[13] Arjmand R, McPherson M. Canada's electricity system transition under alternative policy scenarios. Energy Policy 2022;163:112844. https://doi.org/10.1016/j.enpol.2022.112844.

[14] Colbertaldo P, Parolin F, Campanari S. A comprehensive multi-node multi-vector multi-sector modelling framework to investigate integrated energy systems and assess decarbonisation needs. Energy Convers Manag 2023;291:117168. https://doi.org/10.1016/j.enconman.2023.117168.

[15] Bechara CA, Alnouri SY. Energy assessment strategies in carbon-constrained industrial clusters. Energy Convers Manag 2022;254:115204. https://doi.org/10.1016/j.enconman.2021.115204.

[16] Yazdani H, Baneshi M, Yaghoubi M. Techno-economic and environmental design of hybrid energy systems using multi-objective optimization and multi-criteria decision making methods. Energy Convers Manag 2023;282:116873. https://doi.org/10.1016/j.enconman.2023.116873.

[17] Knöttner S, Leitner B, Hofmann R. Impact of recent district heating developments and low-temperature excess heat integration on design of industrial energy systems: An integrated assessment method. Energy Convers Manag 2022;263.. https://doi.org/10.1016/j.enconman.2022.115612.

[18] Prabhakaran P, Graf F, Koeppel W, Kolb T. Modelling and validation of energy systems with dynamically operated Power to Gas plants for gas-based sector coupling in de-central energy hubs. Energy Convers Manag 2023;276:116534. https://doi.org/10.1016/j.enconman.2022.116534.

[19] Zhang M, Wu Q, Wen J, Lin Z, Fang F, Chen Q. Optimal operation of integrated electricity and heat system: A review of modeling and solution methods. Renew Sustain Energy Rev 2021;135:110098. https://doi.org/10.1016/j.rser.2020.110098.

[20] Lyden A, Pepper R, Tuohy PG. A modelling tool selection process for planning of community scale energy systems including storage and demand side management. Sustain Cities Soc 2018;39:674–88. https://doi.org/10.1016/j.scs.2018.02.003.

[21] Laveneziana L, Prussi M, Chiaramonti D. Critical review of energy planning models for the sustainable development at company level. Energ Strat Rev 2023;49:101136. https://doi.org/10.1016/j.esr.2023.101136.

[22] Allison J, Murphy GB, Counsell JM. Control of micro-CHP and thermal energy storage for minimising electrical grid utilisation. Int J Low-Carbon Technol 2014;11:109–18. https://doi.org/10.1093/ijlct/ctu023.

[23] Franklin GF, Powell JD, Emami-Naeini A. Feedback control of dynamic systems. 6th ed. Upper Saddle River: Prentice Hall: Pearson; 2009.

[24] Diyoke C, Ngwaka U, Ugwu K. A comprehensive analysis on the grid-tied solar photovoltaics for clean energy mix and sup ply in Nigeria's on -grid power. J Energy Syst 2023;7:1–17. https://doi.org/10.30521/jes.988844.

[25] Diyoke C, Ngwaka U. Thermodynamic analysis of a hybrid wind turbine and biomass gasifier for energy supply in a rural off-grid region of Nigeria. Energy Sources Part A 2021;00:1–19. https://doi.org/10.1080/15567036.2021.1922551.

[26] Stewart M, Al-khaykan A, Counsell JM. Assessment of Multi-Domain Energy Systems Modelling Methods. Int J Energy Power Eng 2017;11:832–8.

[27] Shen T, Li Y, Xiang J. A graph-based power flow method for balanced distribution systems. Energies (Basel) 2018;11:1–11. https://doi.org/10.3390/en11030511.

[28] Arif A, Wang Z, Wang J, Mather B, Bashualdo H, Zhao D. Load modeling - A review. IEEE Trans Smart Grid 2018;9:5986–99. https://doi.org/10.1109/TSG.2017.2700436.

[29] Murphy GB, Counsell J, Allison J, Brindley J. Calibrating a combined energy systems analysis and controller design method with empirical data. Energy 2013;57:484–94. https://doi.org/10.1016/j.energy.2013.06.015.

[30] Department for Business, Energy and Industrial Strategy (BEIS) U. Greenhouse gas reporting: conversion factors. 2021. [cited 2023 5 May]; Available from: https://assets.publishing.service.gov.uk/government/uploads/system/uploads/attachment_data/file/1130451/UK_Energy_in_Brief_2022.pdf.

[31] Dowen J, Dowen S, Hammond I, Hill T, Pitcairn N, Webb J. Evaluation of the climate change impacts of waste incineration in. the United Kingdom; 2018.